Available online at www.sciencedirect.com
ScienceDirect
Coordination Chemistry Reviews 252 (2008) 2493–2503
COORDINATION CHEMISTRY REVIEWS
www.elsevier.com/locate/ccr

Review

# Electronic absorption spectroscopy of $[Ru(phen)_2(bpy)]^{2+}$, $[Ru(phen)_2(dmbp)]^{2+}$, $[Ru(tpy)(phen)(CH_3CN)]^{2+}$ and $[Ru(tpy)(dmp)(CH_3CN)]^{2+}$ A theoretical study

Julien Bossert, Chantal Daniel *

*Laboratoire de Chimie Quantique, Institut de Chimie UMR 7177 CNRS, Université Louis Pasteur, 4 Rue Blaise Pascal, 67000 Strasbourg, France*

Received 19 September 2007; accepted 10 February 2008
Available online 16 February 2008

## Contents



## Abstract

The electronic absorption spectroscopy of Ru(II) polyimine complexes, potentially photolabile under visible light irradiation, is investigated by means of density functional theory. The structures of $[Ru(phen)_2(bpy)]^{2+}$, $[Ru(phen)_2(dmbp)]^{2+}$, $[Ru(tpy)(phen)(CH_3CN)]^{2+}$ and $[Ru(tpy)(dmp)(CH_3CN)]^{2+}$ (phen = 1,10-phenanthroline; bpy = 2,2′-bipyridine, tpy = 2,2′; 6′,6″-terpyridine, dmbp = 6,6′-dimethyl-2,2′-bipyridine, dmp = 2,9-dimethyl-1,10-phenanthroline) have been optimized at the DFT(B3LYP) level. The main features of the theoretical absorption spectra of the four molecules have been determined by means of time-dependent DFT (TD-DFT) calculations. The electronic spectra are characterized by a high density of states between 550 nm and 350 nm assigned mainly to metal-to-ligand-charge-transfer (MLCT) states corresponding to electronic excitations to the low-lying π* orbitals, either localised on the phen, dmp and tpy ligands, or delocalised on the phen/bpy, phen/dmbp, phen/tpy and dmp/tpy ligand. The theoretical spectra of $[Ru(phen)_2(dmbp)]^{2+}$ and $[Ru(tpy)(phen)(CH_3CN)]^{2+}$ reproduce rather well the large bands observed experimentally at about 449 nm and 455 nm with a blue shift of 0.2 eV in the latter case. Four $^1$MLCT states ($d_{Ru} \rightarrow \pi^*_{phen}$, $\pi^*_{phen/dmbp}$) calculated at 445 nm, 436 nm, 423 nm and 418 nm with significant oscillator strengths contribute to the band centred at 449 nm in the spectrum of $[Ru(phen)_2(dmbp)]^{2+}$, whereas three $^1$MLCT states ($d_{Ru} \rightarrow \pi^*_{phen}$, $\pi^*_{phen/tpy}$) calculated at 419 nm, 378 nm and 374 nm contribute to the band observed in the spectrum of $[Ru(tpy)(phen)(CH_3CN)]^{2+}$. The theoretical spectrum of $[Ru(phen)_2(bpy)]^{2+}$ does not differ drastically from the spectrum of the analogous dmbp species with four intense, slightly blue-shifted $^1$MLCT ($d_{Ru} \rightarrow \pi^*_{phen}$, $\pi^*_{phen/bpy}$) states, calculated at 432 nm, 429 nm, 408 nm and 395 nm. The theoretical spectrum of $[Ru(tpy)(dmp)(CH_3CN)]^{2+}$ is more compact with close-lying $^1$MLCT states ($d_{Ru} \rightarrow \pi^*_{tpy/dmp}$, $\pi^*_{dmp}$, $\pi^*_{tpy}$) calculated at 428 nm, 424 nm and 416 nm with rather small oscillator strengths. The four complexes are characterized by the presence of potentially dissociative metal centred ($^3$MC) excited states between 400 nm and 350 nm.


*Keywords:* Ruthenium complexes; Theoretical absorption spectra; Time-dependent density functional theory

* Corresponding author.
*E-mail address:* daniel@quantix.u-strasbg.fr (C. Daniel).

0010-8545/$ – see front matter © 2008 Elsevier B.V. All rights reserved.
doi:10.1016/j.ccr.2008.02.005

## 1. Introduction

Ruthenium (II) polyimine complexes have been actively studied in the past 10 years for their photochemical and photophysical properties, which make them remarkable building units in the construction of efficient photoswitchable molecular devices [1–4]. Depending on the coordinated ligands these molecules may behave as photoactive electron/energy transfer components [5] or can undergo photolabilization under UV–vis light. The first process is based on the presence, in the absorption spectrum, of low-lying metal-to-ligand-charge-transfer (MLCT) states whereas the second process is supposed to involve dissociative metal-centred ($^3$MC) excited states accessible via intersystem crossing. For instance irradiation of $[Ru(phen)_2(dmbp)]^{2+}$ and $[Ru(tpy)(phen)(CH_3CN)]^{2+}$ under visible light leads to the clean photo-expulsion of the dimethylbipyridine [1,5] and acetonitrile [6,7], respectively. Efficient photolabilization of $[Ru(phen)_2(dmbp)]^{2+}$ between 300 nm and 800 nm in acetonitrile was observed with formation of $[Ru(phen)_2(CH_3CN)_2]^{2+}$ in a half reaction time of 28 s. This reaction is supposed to be less efficient in the analogous complex $[Ru(phen)_2(bpy)]^{2+}$ [8]. After irradiation of $[Ru(tpy)(phen)(CH_3CN)]^{2+}$ in acetonitrile with large excess of pyridine at 464 nm the $[Ru(tpy)(phen)(py)]^{2+}$ (py = pyridine) is formed with a quantum yield of ∼0.0016. According to the experiments $CH_3CN$ dissociation should be more efficient in the analogous $[Ru(tpy)(dmp)(CH_3CN)]^{2+}$. The photochemical behaviour of these complexes is certainly controlled by the relative position of the $^3$MC states with respect to the absorbing $^1$MLCT states and low-lying $^3$MLCT states. Most of the time the choice of the ligands is determined by qualitative models based on ligand field theory [9].

Most of the theoretical studies devoted to Ru(II) complexes, reported in the recent years, are performed by means of density functional theory. They mainly aim at understanding the electronic structure of Ru(II) polypyridyl complexes used as phototosensitizers in dye-sensitized solar energy cells based on nanostructured $TiO_2$. The first theoretical assignment of the absorption spectrum of $[Ru(bpy)_3]^{2+}$ has shown an important mixing of the excited singlet and triplet states and the transition energies to the MLCT states have been predicted with an accuracy of 1000–2000 $cm^{-1}$ [10]. Following the experiments, a number of theoretical studies have been reported for various molecules where the bpy ligands are substituted by carboxy groups or replaced by cyano/thiocyano ligands to optimize the ability of the complex at sensitizing the semiconductor electrode [11–14]. Another series of Ru(II) complexes, used as luminescent probes of DNA, was recently investigated to determine the structure of the low-lying states involved in this process and to interpret their photophysical behaviour [15–17]. In two recent papers the unusual photophysical properties of Ru(II) polypyridine-type complexes were interpreted with DFT [18,19]. Usually, the agreement between the experimental and TD-DFT theoretical absorption spectra depends strongly on the choice of the functionals, of the basis sets and on the importance of the surrounding effects which may vary from one molecule/solvent system to another one. In addition these various effects may act differently on the ground state and on each type of excited states by over (under)-estimating the transition energies with severe cancellation of errors. These theoretical studies, performed in close connection to the experiments, illustrate the drawbacks of the TD-DFT method, the only one able to handle such large transition metal complexes.

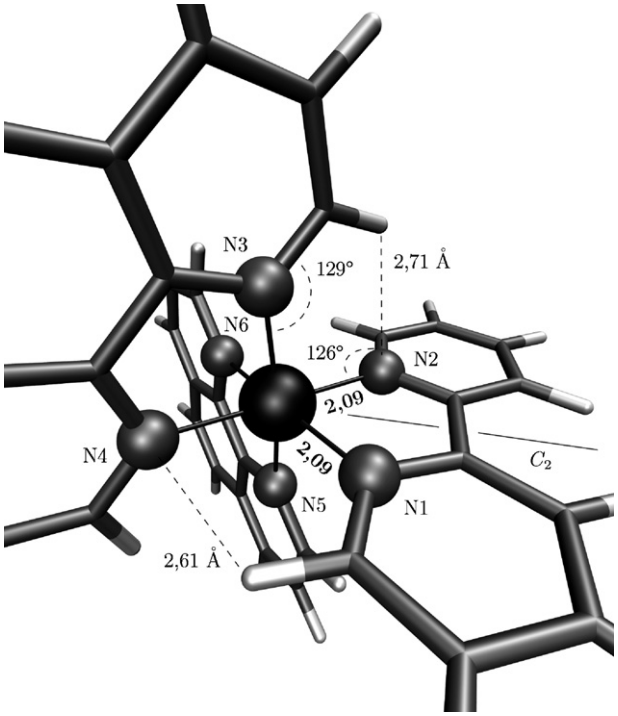


Fig. 1. DFT (B3LYP) optimized structure of $[Ru(phen)_2(bpy)]^{2+}$.

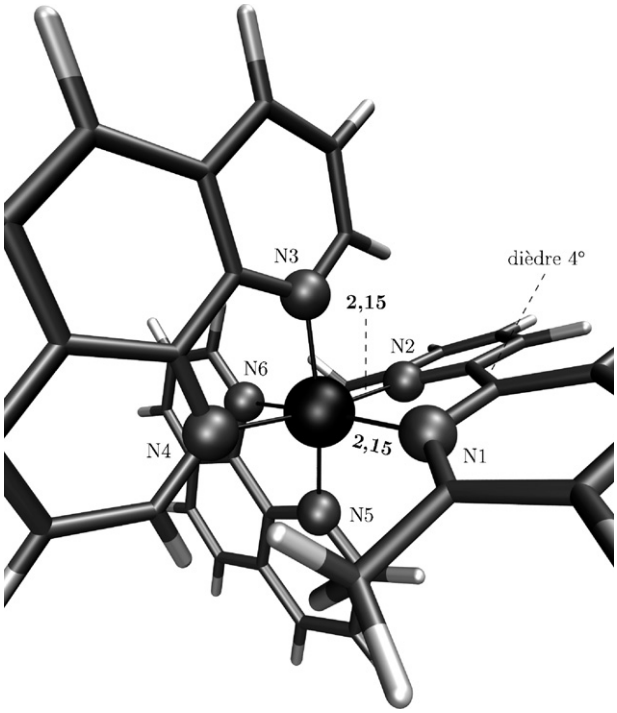


Fig. 2. DFT (B3LYP) optimized structure of $[Ru(phen)_2(dmbp)]^{2+}$.

Table 1
Valence bond lengths and angles of $[Ru(phen)_2(bpy)]^{2+}$ and $[Ru(phen)_2(dmbp)]^{2+}$ (in Å and °)

| $[Ru(phen)_2(bpy)]^{2+}$ | | $[Ru(phen)_2(dmbp)]^{2+}$ | |
|---|---|---|---|
| | Optimized | Optimized | Exp [5] |
| **$Ru–N_1$** | **2.09** | **2.15** | **2.113** |
| **$Ru–N_2$** | **2.09** | **2.15** | **2.100** |
| $Ru–N_3$ | 2.10 | 2.11 | 2.094 |
| $Ru–N_4$ | 2.10 | 2.11 | 2.084 |
| $Ru–N_5$ | 2.10 | 2.09 | 2.077 |
| $Ru–N_6$ | 2.10 | 2.09 | 2.083 |
| $N_1–Ru–N_2$ | 79 | 79 | 78.6 |
| $N_1–Ru–N_3$ | 90 | 87 | |
| $N_1–Ru–N_4$ | 96 | 99 | |
| $N_1–Ru–N_5$ | 96 | 97 | |
| $N_2–Ru–N_3$ | 96 | 92 | |
| $N_2–Ru–N_5$ | 90 | 93 | |
| $N_2–Ru–N_6$ | 96 | 102 | |
| $N_3–Ru–N_4$ | 80 | 79 | 79.0 |
| $N_3–Ru–N_6$ | 96 | 96 | |
| $N_4–Ru–N_5$ | 95 | 96 | |
| $N_4–Ru–N_6$ | 89 | 81 | |
| $N_5–Ru–N_6$ | 80 | 80 | 79.5 |

In order to rationalize and to understand the photochemical behaviour of Ru(II) polyimine complexes, potentially photolabile under visible light irradiation, two of them being characterized experimentally, we propose a semi-quantitative study of the electronic absorption spectroscopy of $[Ru(phen)_2(bpy)]^{2+}$, $[Ru(phen)_2(dmbp)]^{2+}$, $[Ru(tpy)(phen)(CH_3CN)]^{2+}$ and $[Ru(tpy)(dmp)(CH_3CN)]^{2+}$ based on DFT(B3LYP) [20] and TD-DFT [21] calculations. The aim of this work is to determine the geometrical structures and the main features of the electronic absorption spectra as well as to assign the photoactive singlet excited states and the low-lying triplet states.

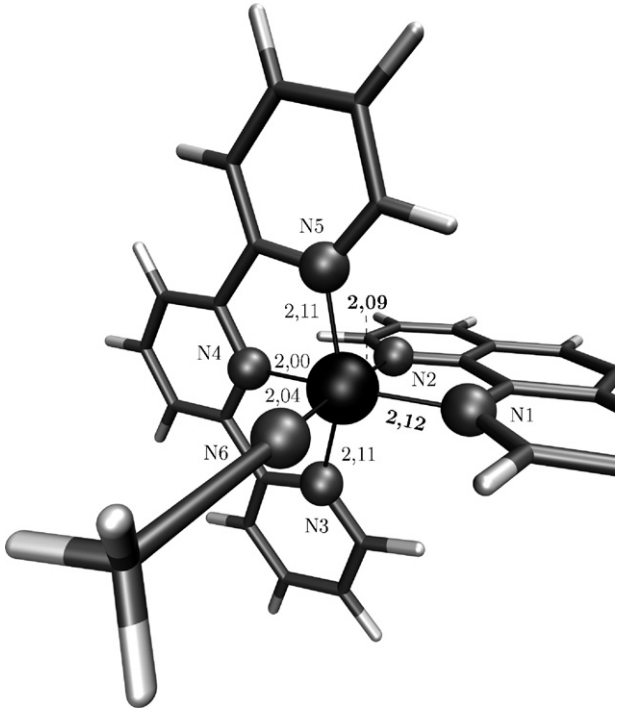


Fig. 3. DFT (B3LYP) optimized structure of $[Ru(tpy)(phen)(CH_3CN)]^{2+}$.

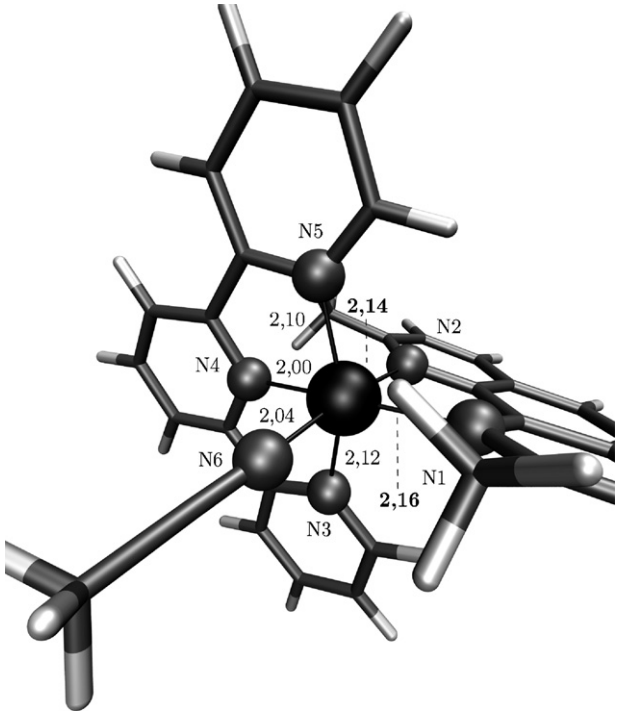


Fig. 4. DFT (B3LYP) optimized structure of $[Ru(tpy)(dmp)(CH_3CN)]^{2+}$.

Table 2
Valence bond lengths and angles of $[Ru(tpy)(phen)(CH_3CN)]^{2+}$ and $[Ru(tpy)(dmp)(CH_3CN)]^{2+}$ (in Å and °)

| $[Ru(tpy)(phen)(CH_3CN)]^{2+}$ | | $[Ru(tpy)(dmp)(CH_3CN)]^{2+}$ | |
|---|---|---|---|
| | Optimized | Optimized | Exp [6] |
| **$Ru–N_1$** | **2.12** | **2.16** | **2.0934** |
| **$Ru–N_2$** | **2.09** | **2.14** | **2.0544** |
| $Ru–N_3$ | 2.11 | 2.12 | 2.0814 |
| $Ru–N_4$ | 2.00 | 2.00 | 1.9734 |
| $Ru–N_5$ | 2.11 | 2.10 | 2.0754 |
| $Ru–N_6$ | 2.04 | 2.04 | 2.0415 |
| $N_1–Ru–N_2$ | 80 | 79 | 79.62 |
| $N_1–Ru–N_3$ | 101 | 100 | 101.12 |
| $N_1–Ru–N_4$ | 175 | 179 | 174.82 |
| $N_1–Ru–N_5$ | 101 | 102 | 99.82 |
| $N_1–Ru–N_6$ | 95 | 97 | 95.82 |
| $N_2–Ru–N_3$ | 91 | 88 | 88.62 |
| $N_2–Ru–N_4$ | 96 | 101 | 95.22 |
| $N_2–Ru–N_5$ | 91 | 95 | 93.32 |
| $N_2–Ru–N_6$ | 174 | 174 | 175.32 |
| $N_3–Ru–N_4$ | 79 | 79 | 79.22 |
| $N_3–Ru–N_5$ | 190 | 159 | 159.02 |
| $N_3–Ru–N_6$ | 90 | 80 | 91.12 |
| $N_4–Ru–N_5$ | 79 | 80 | 79.72 |
| $N_4–Ru–N_6$ | 90 | 83 | 89.32 |
| $N_5–Ru–N_6$ | 90 | 91 | 88.72 |

## 2. Experimental

### 2.1. Computational details

The geometries of $[Ru(phen)_2(bpy)]^{2+}$, $[Ru(phen)_2(dmbp)]^{2+}$, $[Ru(tpy)(phen)(CH_3CN)]^{2+}$ and $[Ru(tpy)(dmp)(CH_3CN)]^{2+}$ were optimized by means of DFT(B3LYP) without symmetry constraint. The metal centre was described by relativistic pseudopotentials ($Z = 16$) and associated valence basis set (8s, 7p, 6d) contracted to [6s, 5p, 3d] [22]. A full double-ξ D95 basis set [9s, 5p] contracted to [4s, 2p] and (4s) contracted to [2s] was used for the second row atoms and for H atoms, respectively [23]. One d function of polarization was added to the basis sets of the second row atoms for the TD-DFT calculation of the theoretical absorption spectra. The optimized structures have been validated by comparison with X-ray data for $[Ru(phen)_2(dmbp)]^{2+}$ [5] and $[Ru(tpy)(dmp)(CH_3CN)]^{2+}$ [6]. The TD-DFT calculations are based on the optimized geometries. The calculations were performed with *Gaussian 03* quantum chemistry software [24]. Solvent effects were not taken into account in the present study. Indeed, we do not believe, at this stage of our investigation, that solvent corrections will modify drastically our conclusion. In a recent article, dedicated to Ru(II) polypyridyl complexes used as intercalators in DNA, we showed that the solvent polarized continuum model (PCM) corrected TD-DFT transition energies for $CH_3CN$, solvent used in the experiments reported here, do not differ significantly from the vacuum values. The maximum shift is a

Table 3
TD-DFT excitation energies (in nm and eV) to the low-lying singlet and triplet states of $[Ru(phen)_2(bpy)]^{2+}$ and associated oscillator strengths ($f$)

| nm | Singlet states | $f$ | Triplet states | eV |
|---|---|---|---|---|
| 532 | | | $^3$MLCT $4d_{Ru} \rightarrow \pi^*_{phen/bpy}$ | 2.33 |
| 529 | | | $^3$MLCT $4d_{Ru} \rightarrow \pi^*_{phen}$ | 2.34 |
| 521 | | | $^3$MLCT $4d_{Ru} \rightarrow \pi^*_{phen/bpy}$ | 2.38 |
| 519 | | | $^3$MLCT $4d_{Ru} \rightarrow \pi^*_{phen}$ | 2.39 |
| 498 | | | $^3$MLCT $4d_{Ru} \rightarrow \pi^*_{phen/bpy}$ | 2.49 |
| 497 | | | $^3$MLCT $4d_{Ru} \rightarrow \pi^*_{phen/bpy}$ | 2.49 |
| 491 | $^1$MLCT $4d_{Ru} \rightarrow \pi^*_{phen/bpy}$ | 0.0 | | 2.52 |
| 480 | | | $^3$MLCT $4d_{Ru} \rightarrow \pi^*_{phen/bpy}$ | 2.58 |
| 475 | $^1$MLCT $4d_{Ru} \rightarrow \pi^*_{phen/bpy}$ | 0.0 | | 2.61 |
| 474 | $^1$MLCT $4d_{Ru} \rightarrow \pi^*_{phen/bpy}$ | 0.0 | | 2.62 |
| 470 | | | $^3$MLCT $4d_{Ru} \rightarrow \pi^*_{phen/bpy}$ | 2.64 |
| 464 | $^1$MLCT $4d_{Ru} \rightarrow \pi^*_{phen/bpy}$ | 0.002 | | 2.67 |
| 462 | | | $^3$MLCT $4d_{Ru} \rightarrow \pi^*_{phen/bpy}$ | 2.68 |
| 448 | $^1$MLCT $4d_{Ru} \rightarrow \pi^*_{phen/bpy}$ | 0.011 | | 2.77 |
| 447 | | | $^3$MLCT $4d_{Ru} \rightarrow \pi^*_{phen}$ | 2.77 |
| 447 | | | $^3$MLCT $4d_{Ru} \rightarrow \pi^*_{phen/bpy}$ | 2.77 |
| 445 | $^1$MLCT $4d_{Ru} \rightarrow \pi^*_{phen/bpy}$ | 0.019 | | 2.78 |
| 433 | | | $^3$MLCT $4d_{Ru} \rightarrow \pi^*_{phen}$ | 2.86 |
| **432** | **$^1$MLCT $4d_{Ru} \rightarrow \pi^*_{phen/bpy}$** | **0.080** | | **2.87** |
| **429** | **$^1$MLCT $4d_{Ru} \rightarrow \pi^*_{phen}$** | **0.074** | | **2.89** |
| 425 | $^1$MLCT $4d_{Ru} \rightarrow \pi^*_{phen}$ | 0.017 | | 2.91 |
| 421 | | | $^3$MLCT $4d_{Ru} \rightarrow \pi^*_{phen}$ | 2.94 |
| 408 | $^1$MLCT $4d_{Ru} \rightarrow \pi^*_{phen}$ | 0.041 | | 3.04 |
| 405 | | | $^3$MLCT/$^3$LLCT $4d_{Ru}/\pi_{phen} \rightarrow \pi^*_{phen}$ | 3.06 |
| 401 | | | $^3$MLCT/$^3$LLCT $4d_{Ru}/\pi_{phen} \rightarrow \pi^*_{phen}$ | 3.09 |
| 400 | $^1$MLCT $4d_{Ru} \rightarrow \pi^*_{phen}$ | 0.011 | | 3.10 |
| 398 | | | $^3$MLCT $4d_{Ru} \rightarrow \pi^*_{phen}$ | 3.11 |
| 395 | $^1$MLCT $4d_{Ru} \rightarrow \pi^*_{phen}$ | 0.076 | | 3.14 |
| 390 | $^1$MLCT $4d_{Ru} \rightarrow \pi^*_{phen}$ | 0.011 | | 3.18 |
| 387 | $^1$MLCT $4d_{Ru} \rightarrow \pi^*_{phen}$ | 0.026 | | 3.20 |
| **383** | | | **$^3$MC $4d_{Ru} \rightarrow 4d_{Ru}$** | **3.23** |
| **381** | | | **$^3$MC $4d_{Ru} \rightarrow 4d_{Ru}$** | **3.26** |
| **380** | | | **$^3$MC $4d_{Ru} \rightarrow 4d_{Ru}$** | **3.26** |
| **379** | | | **$^3$MC $4d_{Ru} \rightarrow 4d_{Ru}$** | **3.27** |
| 377 | $^1$MLCT $4d_{Ru} \rightarrow \pi^*_{phen}$ | 0.027 | | 3.29 |
| 374 | | | $^3$IL $\pi_{phen} \rightarrow \pi^*_{phen}$ | 3.32 |
| 370 | | | $^3$IL $\pi_{phen} \rightarrow \pi^*_{phen}$ | 3.35 |
| 363 | | | $^3$MLCT $4d_{Ru} \rightarrow \pi^*_{bpy}$ | 3.41 |
| 362 | | | $^3$MLCT $4d_{Ru} \rightarrow \pi^*_{bpy}$ | 3.43 |
| 352 | $^1$MLCT $4d_{Ru} \rightarrow \pi^*_{bpy}$ | 0.005 | | 3.52 |

blue shift of 0.13 eV for a $^1$MLCT state which corresponds to a $4d_{Ru} \rightarrow \pi^*_{phen}$ excitation [17]. As illustrated for a series of Ru(II) α-diimine complexes, the influence of the functional on the calculated transition energies may be more dramatic with deviations which may exceed 2.5 eV [25,26]. Finally we would like to point to the fact that solvent corrections are not consistent from one system to another one. In some dramatic situations the solvent correction may compensate the default of DFT at describing the HOMO-LUMO gap for specific charge transfer states involving halides or thiocyanates and the agreement between theoretical and experimental transition energies may be fortuitous.

## 3. Results and discussion

### 3.1. Geometrical structures

The optimized structures of $[Ru(phen)_2(bpy)]^{2+}$ and $[Ru(phen)_2(dmbp)]^{2+}$ are depicted in Figs. 1 and 2, respectively, with selected bond lengths and bond angles collected in Table 1.

The (bpy)$RuN_4$ skeleton of $[Ru(phen)_2(bpy)]^{2+}$ has $C_{2v}$ symmetry with nearly octahedral coordination sphere around the Ru atom. The structure is slightly deformed by the presence of chelates with N–Ru–N angles of 80°. A very small steric effect of the H atoms in 6 and 6′ positions of the bipyridine is

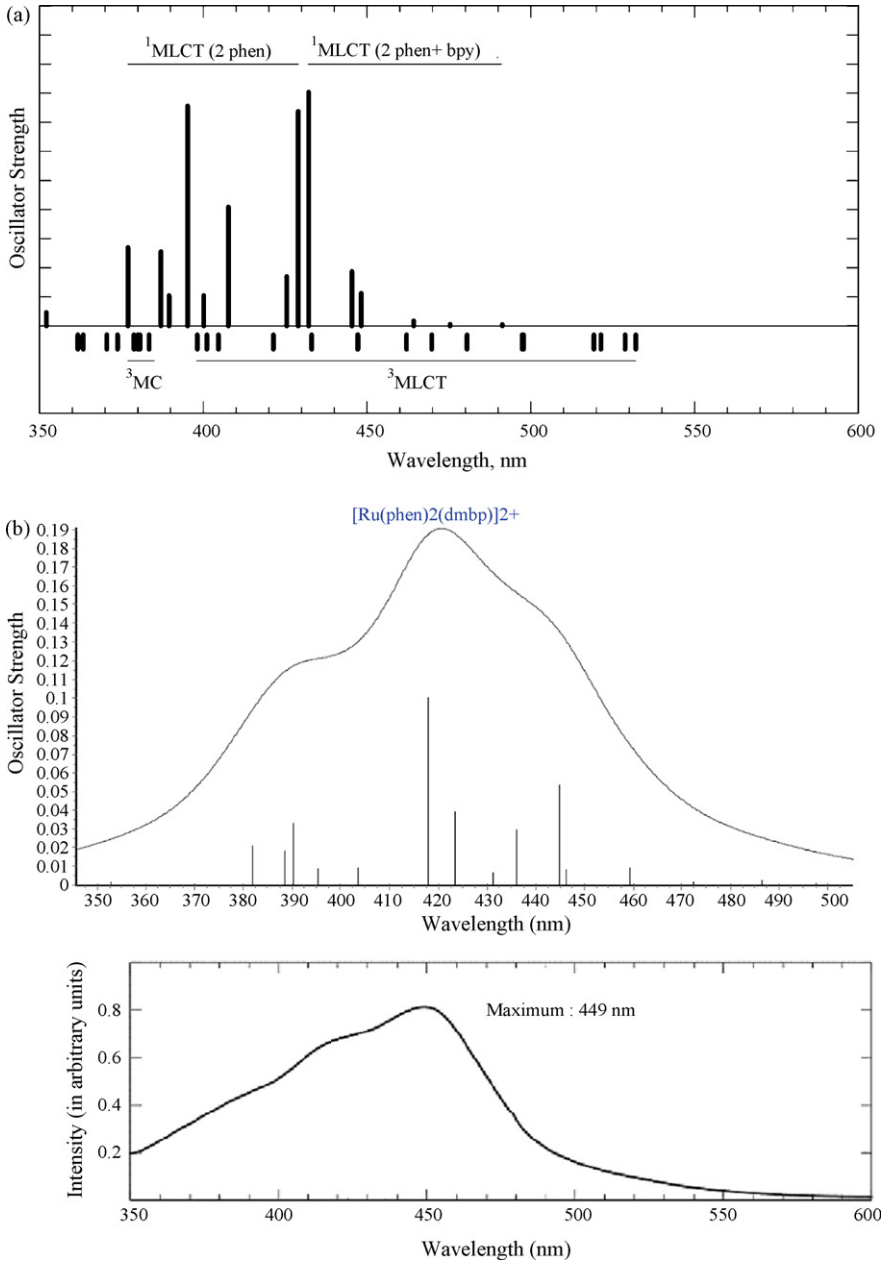


Fig. 5. (a) TD-DFT theoretical absorption spectrum of $[Ru(phen)_2(bpy)]^{2+}$ and (b) TD-DFT theoretical absorption spectrum (top) compared to the experimental one in acetonitrile (bottom) (D. Jouvenot, private communication) of $[Ru(phen)_2(dmbp)]^{2+}$.

observed, bringing closer the phen ligands. The values of the Ru–N distances amount to 2.10 Å (phen) and 2.09 Å (bpy).

The presence of methyl groups in $[Ru(phen)_2(dmbp)]^{2+}$ is responsible for important deformations. One consequence is a significant elongation of the Ru–N bond of the substituted bpy to 2.15 Å (vs. 2.09 Å in bpy) which becomes non-planar with an angle of 4° between the two cycles and out of the $N_1RuN_2$ plane by 14°. The steric effect of the two methyl is the same than the one described above for the H atoms in 6 and 6′ positions, but accentuated, moving the two phen closer with a $N_4RuN_6$ angle of 81° (vs. 89° in $[Ru(phen)_2(bpy)]^{2+}$). The theoretical structure of $[Ru(phen)_2(dmbp)]^{2+}$ agrees rather well with the experimental data obtained for $[Ru(phen)_2(dmbp)]^{2+}(PF_6)^2$ by X-ray [5] and reported in Table 1 for comparison. The bond lengths are slightly overestimated, which is a defect of the B3LYP functional [27]. In particular, the elongation of the Ru–N bonds in dimethylbipyridine with respect to the phenanthroline Ru–N bond lengths is more pronounced in the theoretical geometry (2.15 Å) than in the experimental structure (2.11–2.10 Å).

The theoretical structures of $[Ru(tpy)(phen)(CH_3CN)]^{2+}$ and $[Ru(tpy)(dmp)(CH_3CN)]^{2+}$ are represented in Figs. 3 and 4, respectively. The corresponding optimized bond lengths and bond angles are reported in Table 2.

The coordination sphere is pseudo-octahedral as previously. Because of steric constraints the Ru–$N_4$ bond length between the metal and the central N atom of the tpy ligand is shorter than the other one (2.00 Å vs. 2.09–2.15 Å) (Table 3).

In agreement with the experimental structures based on $[Ru(tpy)(phen)]^{2+}$ $(PF_6)_2$ [6], the Ru–N bond length of the phenanthroline *trans* to the central Ru–$N_4$ bond of the tpy is longer than the *cis* one in both complexes. The values amount to 2.12 Å (*trans*) vs. 2.09 Å (*cis*) in

Table 4
TD-DFT excitation energies (in nm and eV) to the low-lying singlet and triplet states of $[Ru(phen)_2(dmbp)]^{2+}$ and associated oscillator strengths (*f*)

| nm | Singlet states | *f* | Triplet states | eV |
|---|---|---|---|---|
| 548 | | | $^3$MLCT $4d_{Ru} \rightarrow \pi^*_{phen}$ | 2.26 |
| 534 | | | $^3$MLCT $4d_{Ru} \rightarrow \pi^*_{phen/bpy}$ | 2.32 |
| 527 | | | $^3$MLCT $4d_{Ru} \rightarrow \pi^*_{phen/bpy}$ | 2.35 |
| 511 | | | $^3$MLCT $4d_{Ru} \rightarrow \pi^*_{phen/dmbp}$ | 2.42 |
| 500 | | | $^3$MLCT $4d_{Ru} \rightarrow \pi^*_{phen}$ | 2.48 |
| 498 | $^1$MLCT $4d_{Ru} \rightarrow \pi^*_{phen}$ | 0.00 | | 2.49 |
| 487 | $^1$MLCT $4d_{Ru} \rightarrow \pi^*_{phen}$ | 0.003 | | 2.55 |
| 486 | | | $^3$MLCT $4d_{Ru} \rightarrow \pi^*_{phen/bpy}$ | 2.55 |
| 473 | $^1$MLCT $4d_{Ru} \rightarrow \pi^*_{phen/bpy}$ | 0.002 | | 2.62 |
| 472 | | | $^3$MLCT $4d_{Ru} \rightarrow \pi^*_{phen/dmbp}$ | 2.63 |
| 470 | | | $^3$MLCT $4d_{Ru} \rightarrow \pi^*_{phen/dmbp}$ | 2.64 |
| 459 | | | $^3$MLCT $4d_{Ru} \rightarrow \pi^*_{phen}$ | 2.70 |
| 459 | $^1$MLCT $4d_{Ru} \rightarrow \pi^*_{phen}$ | 0.009 | | 2.70 |
| 452 | | | $^3$MLCT $4d_{Ru} \rightarrow \pi^*_{dmbp}$ | 2.74 |
| 446 | $^1$MLCT $4d_{Ru} \rightarrow \pi^*_{phen/dmbp}$ | 0.008 | | 2.78 |
| **445** | **$^1$MLCT $4d_{Ru} \rightarrow \pi^*_{phen/dmbp}$** | **0.053** | | **2.79** |
| 445 | | | $^3$MLCT $4d_{Ru} \rightarrow \pi^*_{dmbp}$ | 2.79 |
| 437 | | | $^3$MLCT $4d_{Ru} \rightarrow \pi^*_{dmbp}$ | 2.84 |
| **436** | **$^1$MLCT $4d_{Ru} \rightarrow \pi^*_{phen}$** | **0.029** | | **2.84** |
| 435 | | | $^3$MLCT $4d_{Ru} \rightarrow \pi^*_{dmbp}$ | 2.85 |
| 431 | $^1$MLCT $4d_{Ru} \rightarrow \pi^*_{phen/bpy}$ | 0.007 | | 2.87 |
| 424 | | | $^3$MLCT/$^3$IL | 2.93 |
| **423** | **$^1$MLCT $4d_{Ru} \rightarrow \pi^*_{phen/dmbp}$** | **0.039** | | **2.93** |
| **418** | **$^1$MLCT $4d_{Ru} \rightarrow \pi^*_{phen}$** | **0.100** | | **2.97** |
| 417 | | | $^3$MC/$^3$IL $4d_{Ru}/\pi_{phen} \rightarrow \pi^*_{phen}$ | 2.97 |
| 405 | | | $^3$MLCT $4d_{Ru} \rightarrow \pi^*_{phen}$ | 3.06 |
| 404 | $^1$MLCT $4d_{Ru} \rightarrow \pi^*_{phen}$ | 0.009 | | 3.07 |
| 401 | | | $^3$MC/$^3$MLCT $4d_{Ru} \rightarrow 4d_{Ru}/\pi^*_{phen}$ | 3.09 |
| **396** | | | **3 MC $4d_{Ru} \rightarrow 4d_{Ru}$** | **3.13** |
| 396 | $^1$MLCT $4d_{Ru} \rightarrow \pi^*_{phen}$ | 0.008 | | 3.13 |
| **391** | | | **3 MC $4d_{Ru} \rightarrow 4d_{Ru}$** | **3.17** |
| 390 | $^1$MLCT $4d_{Ru} \rightarrow \pi^*_{phen}$ | 0.033 | | 3.18 |
| 389 | $^1$MLCT $4d_{Ru} \rightarrow \pi^*_{phen}$ | 0.018 | | 3.19 |
| **387** | | | **$^3$MC $4d_{Ru} \rightarrow 4d_{Ru}$** | **3.21** |
| 382 | $^1$MLCT $4d_{Ru} \rightarrow \pi^*_{phen/bpy}$ | 0.021 | | 3.25 |
| 382 | | | $^3$MC/$^3$MLCT $4d_{Ru} \rightarrow 4d_{Ru}/\pi^*_{phen}$ | 3.25 |
| **378** | | | **$^3$MC $4d_{Ru} \rightarrow 4d_{Ru}$** | **3.28** |
| 353 | $^1$MLCT/$^1$MC $4d_{Ru} \rightarrow \pi^*_{dmbp}/4d_{Ru}$ | 0.002 | | 3.51 |

$[Ru(tpy)(phen)(CH_3CN)]^{2+}$ and 2.16 Å (*trans*) vs. 2.14 Å (*cis*) in the more crowded methyl-substituted phenanthroline complex $[Ru(tpy)(dmp)(CH_3CN)]^{2+}$. The bond lengths are overestimated with respect to the experimental values by about 0.03 Å except for the Ru–$N_6$ bond length between the metal and the acetonitrile. In contrast to $[Ru(phen)_2(dmbp)]^{2+}$ the substituted phenanthroline remains planar because of less flexibility. However, an out of plane deformation is also observed.

### 3.2. Electronic absorption spectroscopy

The main features of the theoretical absorption spectra of $[Ru(phen)_2(bpy)]^{2+}$ and $[Ru(phen)_2(dmbp)]^{2+}$ are represented in Fig. 5a and b, respectively, where the details on the transitions energies, oscillator strengths and assignments are given in Tables 3 and 4.

The absorption spectrum of $[Ru(phen)_2(bpy)]^{2+}$ is characterized by 12 singlet states with significant oscillator strengths (greater than 0.01) ranging between 450 nm and 380 nm, namely within an energy domain of ~1 eV. These excited states correspond to MLCT states with a charge transfer delocalised on both phen ligands. In the lowest states the delocalisation is extended to the bpy ligand. The main features of the theoretical spectrum are the presence of three strongly absorbing $^1$MLCT states at 432 nm (2.87 eV), 429 nm (2.89 eV) and 395 nm (3.14 eV).

Fig. 6a represents the contour plot of electronic density differences between the electronic ground state and the MLCT states calculated at 448 nm (left side) and 395 nm (right side). The light densities correspond to a decrease in electronic density and the dark one to an increase illustrating clearly the metal-to-ligand-charge-transfer nature of these two states. Interestingly, the delocalised character over the ligands, observed in the Franck–Condon region (Fig. 6a) before any nuclear structural rearrangement, is not inconsistent with the idea of localised excited states in this class of complexes [28,29]. Indeed, after absorption the molecular structure will evolve in less than 100 fs via vibrational relaxation in the singlet-excited state. Depending on the relative position of the singlet and triplet states in the FC region more or less fast intersystem crossings (from a few tens of fs to ps) to the long life time triplet excited states will occur. This standard deactivation mechanism will be accompanied by localisation on a single ligand as in the $[Ru(bpy)_3]^{2+}$ complex [28]. For an interesting discussion on the localised/delocalised description the reader is refereed to Ref. [19].

The corresponding $^3$MLCT states range between 398 nm, whereas a series of $^3$MC states is found between 383 nm and 379 nm. Two nearly degenerate triplet states calculated at 405 nm and 401 nm possess mixed MLCT/LLCT character with a significant contribution of bpy to phen charge transfer character.

The theoretical absorption spectrum of $[Ru(phen)_2(dmbp)]^{2+}$ is compared to the experimental spectrum of $[Ru(phen)_2(dmbp)]^{2+}(PF_6)_2$ obtained in acetonitrile (Fig. 5b). Several $^1$MLCT states contribute to the intense band centred at 449 nm, two are calculated at 445 nm ($f$ = 0.0534) and 423 nm ($f$ = 0.0389) and are delocalised over the phen and dmbp ligands,

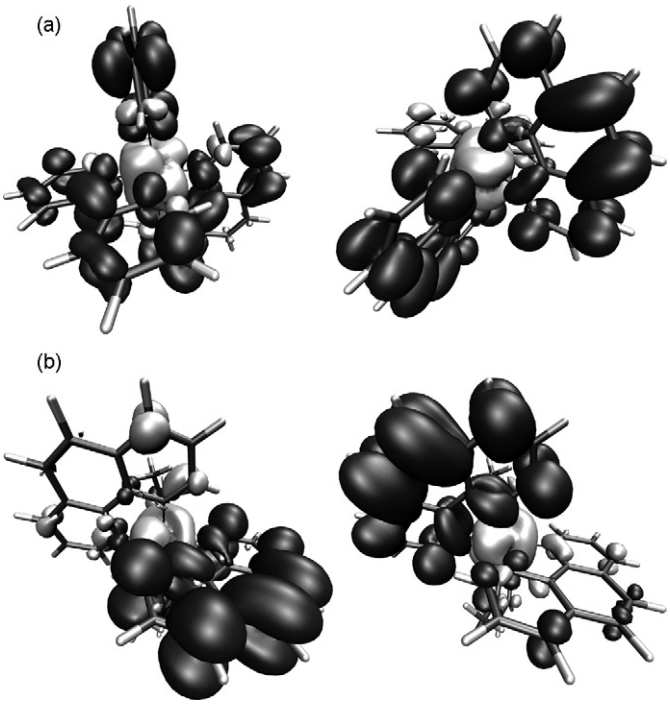


Fig. 6. (a) Electronic density difference isosurfaces ($5 \times 10^{-4}$ a.u.) between the electronic ground state and the low-lying singlet MLCT excited states of $[Ru(phen)_2(bpy)]^{2+}$ calculated at 448 nm (left side) and 395 nm (right side) and (b) electronic density difference isosurfaces ($5 \times 10^{-4}$ a.u.) between the electronic ground state and the low-lying singlet MLCT excited states of $[Ru(phen)_2(dmbp)]^{2+}$ calculated at 390 nm (left side) and 389 nm (right side). The dark and light volumes correspond to an increase and a decrease of density, respectively.

the two others are calculated at 436 nm ($f$ = 0.0293) and 418 nm ($f$ = 0.1) and correspond to charge transfer to one phen. The theoretical spectrum in gas phase is shifted to the blue by about 0.20 eV with respect to the experimental spectrum observed in solvent.

The corresponding transition energies and oscillator strengths are reported in Table 4. The main difference between the theoretical spectra of $[Ru(phen)_2(bpy)]^{2+}$ and $[Ru(phen)_2(dmbp)]^{2+}$ is the MLCT states localisation. This is illustrated by the contour plot of electronic density differences between the electronic ground state and the MLCT states calculated at 390 nm (left side) and 389 nm (right side) (Fig. 6b) where the density is localised on one phen ligand, only. This is mainly a consequence of the loss of symmetry due to the steric constraint of the methyl groups. The upper part of the spectrum is characterized by the presence of a number of $^3$MC states between 417 nm and 378 nm.

The main characteristic of the theoretical absorption spectra of both complexes is a high density of states within 1.0 eV or 8000 $cm^{-1}$ with more than 10 singlet states with significant oscillator strengths (0.007–0.1) between 440 nm and 480 nm. The increase of the Ru–N bond distances when replacing the bpy ligand by the dmbp ligand has some significant influence on the position of the $^3$MC states. Whereas the spectrum of $[Ru(phen)_2(bpy)]^{2+}$ is characetrized by four triplet states centred on the metal between 379 nm and 383 nm, in

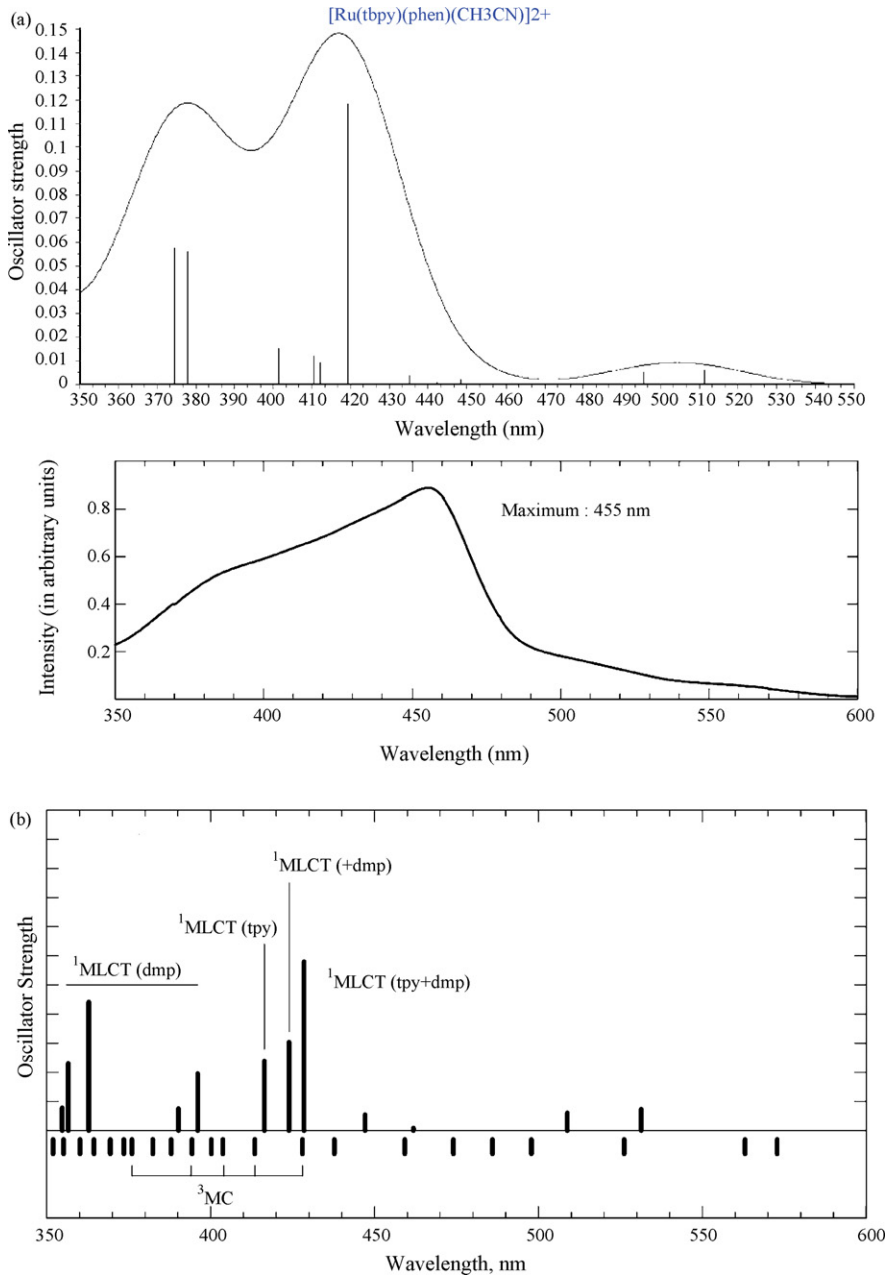


Fig. 7. (a) TD-DFT theoretical absorption spectrum (top) as compared to the experimental one in acetonitrile (bottom) (S. Bonnet, private communication) of $[Ru(tpy)(phen)(CH_3CN)]^{2+}$ and (b) TD-DFT theoretical absorption spectrum of $[Ru(tpy)(dmp)(CH_3CN)]^{2+}$.

$[Ru(phen)_2(dmbp)]^{2+}$ all the upper states above 420 nm correspond to $^3$MC states.

The main features of the theoretical absorption spectra of $[Ru(tpy)(phen)(CH_3CN)]^{2+}$ and $[Ru(tpy)(dmp)(CH_3CN)]^{2+}$ are represented in Fig. 7a and b where the transition energies, oscillator strengths and assignments are given in Tables 5 and 6, respectively.

The theoretical absorption spectrum of $[Ru(tpy)(phen)(CH_3CN)]^{2+}$ is compared to the experimental spectrum observed in acetonitrile (Fig. 7a). The singlet excited states correspond to $^1$MLCT states with charge transfer either to the phen or to the tpy. Three states calculated at 419 nm, 378 nm and 374 nm have significant oscillator strengths and contribute to the large experimental band starting at 350 nm with a maximum centred at 455 nm. The maximum may be attributed to a charge transfer from Ru to the tpy/phen ligands and the shoulder at about 385 nm to a charge transfer to the phen. As for $[Ru(phen)_2(dmp)]^{2+}$ the theoretical spectrum is slightly shifted to the blue with respect to the experimental one. Three $^3$MC states are calculated at 397 nm, 378 nm and 355 nm.

The theoretical spectrum of $[Ru(tpy)(dmp)(CH_3CN)]^{2+}$ (Fig. 7b and Table 6) is red shifted with respect to the spectrum of $[Ru(tpy)(phen)(CH_3CN)]^{2+}$. The most intense band corresponds to a charge transfer from Ru to tpy/dmp calculated at 428 nm ($f = 0.058$). Again the presence of methyl groups has some influence on the occurrence of low-lying triplet MC states between

Table 5
TD-DFT excitation energies (in nm and eV) to the low-lying singlet and triplet states of $[Ru(tpy)(phen)(CH_3CN)]^{2+}$ and associated oscillator strengths (*f*)

| nm | Singlet states | *f* | Triplet states | eV |
|---|---|---|---|---|
| 548 | | | $^3$MLCT $4d_{Ru} \rightarrow \pi^*_{tpy}$ | 2.26 |
| 543 | | | $^3$MLCT $4d_{Ru} \rightarrow \pi^*_{tpy}$ | 2.28 |
| 518 | | | $^3$MLCT $4d_{Ru} \rightarrow \pi^*_{tpy}$ | 2.39 |
| 511 | $^1$MLCT $4d_{Ru} \rightarrow \pi^*_{tpy}$ | 0.006 | | 2.42 |
| 508 | | | $^3$MLCT $4d_{Ru} \rightarrow \pi^*_{phen}$ | 2.44 |
| 496 | $^1$MLCT $4d_{Ru} \rightarrow \pi^*_{tpy}$ | 0.005 | | 2.50 |
| 495 | | | $^3$MLCT $4d_{Ru} \rightarrow \pi^*_{phen}$ | 2.51 |
| 480 | | | $^3$MLCT $4d_{Ru} \rightarrow \pi^*_{tpy}$ | 2.58 |
| 449 | $^1$MLCT $4d_{Ru} \rightarrow \pi^*_{tpy}$ | 0.002 | | 2.76 |
| 444 | | | $^3$MLCT $4d_{Ru} \rightarrow \pi^*_{tpy}$ | 2.79 |
| 442 | $^1$MLCT $4d_{Ru} \rightarrow \pi^*_{phen}$ | 0.001 | | 2.80 |
| 438 | | | $^3$MLCT $4d_{Ru} \rightarrow \pi^*_{phen}$ | 2.83 |
| 437 | | | $^3$MLCT $4d_{Ru} \rightarrow \pi^*_{tpy}$ | 2.84 |
| 435 | $^1$MLCT $4d_{Ru} \rightarrow \pi^*_{tpy}$ | 0.004 | | 2.85 |
| **419** | **$^1$MLCT $4d_{Ru} \rightarrow \pi^*_{tpy/phen}$** | **0.118** | | **2.96** |
| 418 | | | $^3$MLCT $4d_{Ru} \rightarrow \pi^*_{phen}$ | 2.96 |
| 412 | $^1$MLCT $4d_{Ru} \rightarrow \pi^*_{phen}$ | 0.009 | | 3.01 |
| 411 | $^1$MLCT $4d_{Ru} \rightarrow \pi^*_{tpy}$ | 0.012 | | 3.02 |
| 404 | | | $^3$MLCT $4d_{Ru} \rightarrow \pi^*_{phen}$ | 3.07 |
| 402 | $^1$MLCT $4d_{Ru} \rightarrow \pi^*_{phen}$ | 0.015 | | 3.09 |
| **397** | | | **$^3$MC $4d_{Ru} \rightarrow 4d_{Ru}$** | **3.12** |
| 396 | | | $^3$IL $\pi_{tpy} \rightarrow \pi^*_{tpy}$ | 3.13 |
| 386 | | | $^3$IL $\pi_{tpy} \rightarrow \pi^*_{tpy}$ | 3.21 |
| 378 | $^1$MLCT $4d_{Ru} \rightarrow \pi^*_{phen}$ | 0.056 | | 3.28 |
| **378** | | | **$^3$MC $4d_{Ru} \rightarrow 4d_{Ru}$** | **3.28** |
| 374 | $^1$MLCT $4d_{Ru} \rightarrow \pi^*_{phen}$ | 0.057 | | 3.31 |
| 373 | | | $^3$MLCT $4d_{Ru} \rightarrow \pi^*_{phen}$ | 3.32 |
| 369 | | | $^3$IL $\pi_{phen} \rightarrow \pi^*_{phen}$ | 3.36 |
| 368 | | | $^3$MLCT $4d_{Ru} \rightarrow \pi^*_{phen}$ | 3.37 |
| 367 | $^1$MLCT $4d_{Ru} \rightarrow \pi^*_{phen}$ | 0.000 | | 3.38 |
| **355** | | | **$^3$MC $4d_{Ru} \rightarrow 4d_{Ru}$** | **3.49** |
| 354 | | | $^3$MLCT $4d_{Ru} \rightarrow \pi^*_{tpy}$ | 3.51 |
| 352 | | | $^3$IL $\pi_{phen} \rightarrow \pi^*_{phen}$ | 3.52 |

428 nm and 376 nm. The degeneracy between the lowest $^3$MC state and the $^1$MLCT absorbing state calculated at 428 nm will have dramatic influence on the photodissociation mechanism of the acetonitrile from $[Ru(tpy)(dmp)(CH_3CN)]^{2+}$ derivatives.

### 3.3. State correlation diagrams for the photodissociation of $CH_3CN$

The state diagrams which correlate the electronic ground and excited states of the complexes $[Ru(tpy)(L)(CH_3CN)]^{2+}$ (L = phen or dmp) to the fragments $[Ru(tpy(L)]^{2+}$ are represented in Fig. 8a (L = phen) and b (L = dmp). It was supposed that the photodissociation of $CH_3CN$ is faster than the molecules and solvent relaxation in line with a dissociative mechanism where the rate-determining step is the acetonitrile dissociation. This hypothesis is consistent with the mechanism proposed experimentally for the photosubstitution in Ru(II) polyimine complexes [30–32].

The order and the character of the low-lying excited states in the two fragments are similar but the energetics is different. In both molecules two sets of $^1$MC (within 0.3 eV) and $^3$MC (within 0.3 eV) states are separated by about 0.5 eV. These sets are followed by a high density of $^{1,3}$MLCT states within 1.0 eV. In both complexes the $^3$MC states are dissociative leading to $[Ru(tpy)(phen)]^{2+}$ and $[Ru(tpy)(dmp)]^{2+}$ in a $^3$MC state at 0.95 eV and 0.75 eV above the singlet ground state, respectively. According to the qualitative picture depicted in Fig. 8a and b the $^3$MC potential energy curve is steeper in the case of the dmp-substituted complex. Moreover, the lowest $^3$MC state of this molecule, calculated at 413 nm, is nearly degenerated with the $^1$MLCT absorbing states calculated between 428 nm and 416 nm and more easily accessible upon visible irradiation. All these features are in favour of a more efficient photodissociation of $CH_3CN$ in $[Ru(tpy)(dmp)(CH_3CN)]^{2+}$ than in $[Ru(tpy)(phen)(CH_3CN]^{2+}$ as expected from experiments [7].

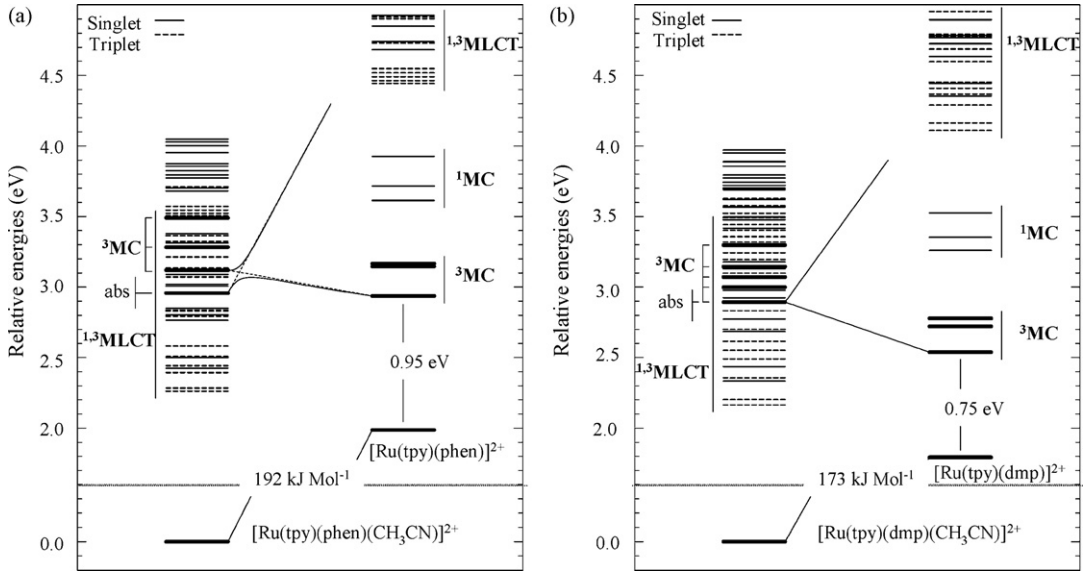


Fig. 8. (a) State correlation diagrams for the photodissociation of $CH_3CN$ from $[Ru(tpy)(phen)(CH_3CN)]^{2+}$ and (b) state correlation diagrams for the photodissociation of $CH_3CN$ from $[Ru(tpy)(dmp)(CH_3CN)]^{2+}$.

Table 6
TD-DFT excitation energies (in nm and eV) to the low-lying singlet and triplet states of $[Ru(tpy)(dmp)(CH_3CN)]^{2+}$ and associated oscillator strengths (*f*)

| nm | Singlet states | *f* | Triplet states | eV |
|---|---|---|---|---|
| 573 | | | $^3$MLCT $4d_{Ru} \rightarrow \pi^*_{tpy}$ | 2.16 |
| 563 | | | $^3$MLCT $4d_{Ru} \rightarrow \pi^*_{tpy}$ | 2.20 |
| 531 | $^1$MLCT $4d_{Ru} \rightarrow \pi^*_{tpy}$ | 0.007 | | 2.33 |
| 526 | | | $^3$MLCT $4d_{Ru} \rightarrow \pi^*_{tpy}$ | 2.36 |
| 509 | $^1$MLCT $4d_{Ru} \rightarrow \pi^*_{tpy}$ | 0.006 | | 2.44 |
| 498 | | | $^3$MLCT $4d_{Ru} \rightarrow \pi^*_{tpy}$ | 2.49 |
| 486 | | | $^3$MLCT $4d_{Ru} \rightarrow \pi^*_{dmp}$ | 2.55 |
| 474 | | | $^3$MLCT $4d_{Ru} \rightarrow \pi^*_{dmp}$ | 2.62 |
| 462 | $^1$MLCT $4d_{Ru} \rightarrow \pi^*_{tpy}$ | 0.001 | | 2.68 |
| 459 | | | $^3$MLCT $4d_{Ru} \rightarrow \pi^*_{tpy}$ | 2.70 |
| 447 | $^1$MLCT $4d_{Ru} \rightarrow \pi^*_{tpy}$ | 0.006 | | 2.77 |
| 438 | | | $^3$MLCT $4d_{Ru} \rightarrow \pi^*_{tpy}$ | 2.83 |
| **428** | **$^1$MLCT $4d_{Ru} \rightarrow \pi^*_{tpy/dmp}$** | **0.058** | | **2.89** |
| 428 | | | $^3$MC/$^3$MLCT $4d_{Ru} \rightarrow 4d_{Ru}/\pi^*_{tpy}$ | 2.90 |
| **424** | **$^1$MLCT $4d_{Ru} \rightarrow \pi^*_{dmp}$** | **0.030** | | **2.92** |
| **416** | **$^1$MLCT $4d_{Ru} \rightarrow \pi^*_{tpy}$** | **0.024** | | **2.98** |
| **413** | | | **$^3$MC $4d_{Ru} \rightarrow 4d_{Ru}$** | **3.00** |
| **404** | | | **$^3$MC/$^3$MLCT $4d_{Ru} \rightarrow 4d_{Ru}/\pi^*_{dmp}$** | **3.07** |
| 400 | | | $^3$IL $\pi_{dmp} \rightarrow \pi^*_{dmp}$ | 3.10 |
| 396 | $^1$MLCT $4d_{Ru} \rightarrow \pi^*_{dmp}$ | 0.020 | | 3.13 |
| **394** | | | **$^3$MC $4d_{Ru} \rightarrow 4d_{Ru}$** | **3.14** |
| 390 | $^1$MLCT $4d_{Ru} \rightarrow \pi^*_{dmp}$ | 0.008 | | 3.18 |
| 388 | | | $^3$IL $\pi_{tpy} \rightarrow \pi^*_{tpy}$ | 3.20 |
| 382 | | | $^3$MLCT $4d_{Ru} \rightarrow \pi^*_{dmp}$ | 3.24 |
| **376** | | | **$^3$MC $4d_{Ru} \rightarrow 4d_{Ru}$** | **3.30** |
| 374 | | | $^3$IL $\pi_{dmp} \rightarrow \pi^*_{dmp}$ | 3.32 |
| 369 | | | $^3$IL/$^3$MLCT $\pi_{dmp}/4d_{Ru} \rightarrow \pi^*_{dmp}$ | 3.36 |
| 364 | | | $^3$MLCT $4d_{Ru} \rightarrow \pi^*_{dmp}$ | 3.40 |
| 363 | $^1$MLCT $4d_{Ru} \rightarrow \pi^*_{dmp}$ | 0.044 | | 3.42 |
| 360 | | | $^3$MLCT $4d_{Ru} \rightarrow \pi^*_{tpy}$ | 3.44 |
| 357 | $^1$MLCT $4d_{Ru} \rightarrow \pi^*_{dmp}$ | 0.023 | | 3.48 |
| 355 | | | $^3$LLCT $\pi^*_{phen} \rightarrow \pi^*_{tpy}$ | 3.49 |
| 355 | $^1$MLCT $4d_{Ru} \rightarrow \pi^*_{tpy}$ | 0.008 | | 3.50 |

## 4. Summary

The geometries of four Ru(II) polyimine complexes have been investigated by means of DFT(B3LYP). It was shown that these complexes keep their nearly octahedral structure and are somewhat rigid. The electronic absorption in the visible and near UV is due essentially to MLCT excited states towards the polyimine ligands. These complexes are characterized by a high density of states within 1.0 eV but only a few MLCT states have significant oscillator strengths. These MLCT states are rather delocalised either over the phen/bpy and phen/dmbp in $[Ru(phen)_2(bpy)]^{2+}$ and $[Ru(phen)_2(dmbp)]^{2+}$or over the phen/tpy and tpy/dmp in $[Ru(tpy)(phen)(CH_3CN)]^{2+}$ and $[Ru(tpy)(dmp)(CH_3CN)]^{2+}$. The MLCT character and the delocalisation are well illustrated by electronic density differences between the ground state and some of the absorbing MLCT states. This picture is not in contradiction with the localisation on a single ligand put in evidence in long time scale experiments. Indeed localisation occurs in the long life time triplet excited states populated via intersystem crossing from the $^1$MLCT absorbing states. In agreement with simple ligand field theory, substitution of the polyimines ligands by methyl groups will increase the Ru–N bond lengths and lower the metal centred states. One important conclusion is the near degeneracy of the lowest $^3$MC states with some of the low-lying $^1$MLCT states in the case of $[Ru(tpy)(dmp)(CH_3CN)]^{2+}$. This element is probably the key of the photodissociation mechanism of acetonitrile in this molecule and derivatives. Before going further into the theoretical investigation of this class of molecules, validation of the computational method has to be performed. Solvent corrections cannot simply be added via a crude model which may bias the response of the TD-DFT by moving artificially the relative positions of some important Kohn–Sham orbitals.

## Acknowledgements

The authors gratefully thank J.P. Collin, D. Jouvenot and S. Bonnet for helpful discussions and private communications. The calculations were carried out in part at the centre Universitaire et Régional de Ressources Informatiques (CURRI, Université Louis Pasteur, Strasbourg), in part at the IDRIS computer cen-

tre (CNRS, Orsay) through a grant of computer time from the Conseil Scientifique and at the LCQS (Strasbourg).

## References

[1] A.C. Laemmel, J.P. Collin, J.P. Sauvage, Eur. J. Inorg. Chem. 1999 (1999) 383.
[2] E. Baranoff, J.P. Collin, Y. Furusho, A.C. Laemmel, J.P. Sauvage, Chem. Commun. 2000 (2000) 1935.
[3] J.P. Collin, A.C. Laemmel, J.P. Sauvage, New J. Chem. 25 (2001) 22.
[4] A. Juris, V. Balzani, Coord. Chem. Rev. 84 (1988) 85.
[5] E. Baranoff, J.P. Collin, J. Furusho, Y. Furusho, A.C. Laemmel, J.P. Sauvage, Inorg. Chem. 41 (2002) 1215.
[6] S. Bonnet, J.P. Collin, N. Gruber, J.P. Sauvage, E.R. Schofield, Dalton Trans. 2003 (2003) 4654.
[7] S. Bonnet, J.P. Collin, J.P. Sauvage, E.R. Schofield, Inorg. Chem. 43 (2004) 8346.
[8] B. Durham, B.J.V. Caspar, J.K. Nagle, T.J. Meyer, J. Am. Chem. Soc. 104 (1982) 4803.
[9] D.W. Smith, Ligand field theory and spectra, in: R.B. King (Ed.), Encyclopedia of Inorganic Chemistry, vol. 4, J. Wiley & Sons, 1994, pp. 1965–1982.
[10] C. Daul, E.J. Baerends, P. Vernooijs, Inorg. Chem. 33 (1994) 3538.
[11] J.F. Guillemoles, V. Barone, L. Joubert, C. Adamo, J. Phys. Chem. A 106 (2002) 11354.
[12] J.E. Monat, J.H. Rodriguez, J.K. McCusker, J. Phys. Chem. A 106 (2002) 7399.
[13] S. Fantacci, F. De Angelis, A. Selloni, J. Am. Chem. Soc. 125 (2003) 4381.
[14] Y. Xu, W.-K. Chen, M.-J. Cao, S.-H. Liu, J.-Q. Li, A.I. Philippopoulos, P. Falaras, Chem. Phys. 330 (2006) 204.
[15] E.R. Batista, R.L. Martin, J. Phys. Chem. A 109 (2005) 3128.
[16] F. Alary, J.-L. Heully, L. Bijeire, P. Vicendo, Inorg. Chem. 46 (2007) 3154.
[17] M. Atsumi, L. González, C. Daniel, J. Photochem. Photobiol. A: Chem. 190 (2007) 310.
[18] M.-F. Charlot, A. Aukauloo, J. Phys. Chem. A 111 (2007) 11661.
[19] M.-F. Charlot, Y. Pellegrin, A. Quaranta, W. Leibl, A. Aukauloo, Chem. A: Eur. J. 12 (2006) 796.
[20] C. Lee, W. Yang, R.G. Parr, Phys. Rev. B 37 (1988) 785;
A.D. Becke, J. Chem. Phys. 98 (1993) 5648.
[21] C. Jamorski, M.E. Casida, D.R. Salahub, J. Chem. Phys. 104 (1996) 5134.
[22] D. Andrae, U. Haeussermann, M. Dolg, H. Stoll, H. Preuss, Theor. Chim. Acta 77 (1990) 123.
[23] T.H.J. Dunning, P.J. Hay, Gaussian basis sets for molecular calculations, in: H.F. Schaefer III (Ed.), Methods for Electronic Structure Theory, New York Plenum, 1977, pp. 1–28.
[24] M.J. Frisch, et al., Gaussian 03, Gaussian, Inc., Pittsburgh, PA, 2003.
[25] N. Ben Amor, S. Záliš, C. Daniel, Int. J. Quant. Chem. 106 (2006) 2458.
[26] S. Záliš, N. Ben Amor, C. Daniel, Inorg. Chem. 43 (2004) 7978.
[27] M. Buchs, C. Daul, Chimia 52 (1998) 163.
[28] N.H. Damrauer, G. Cerullo, A. Yeh, T.R. Boussie, C.V. Shank, J.K. McCusker, Science 275 (1997) 54.
[29] M. Saes, C. Bressler, R. Abela, D. Grolimund, S.L. Johnson, P.A. Heinmann, M. Chergui, Phys. Rev. Lett. 90 (2003) 047403.
[30] F.-F. Suen, S.W. Wilson, M. Pomerantz, J.L. Walsh, Inorg. Chem. 28 (1989) 786.
[31] C.R. Hecker, P.E. Fanwick, D.R. McMillin, Inorg. Chem. 30 (1991) 659.
[32] A.-C. Laemmel, J.-P. Collin, J.-P. Sauvage, C.R. Acad. Sci. Paris, Sér. IIc Chim. 3 (2000) 43.